

Junction dynamics in phase-field simulations vis-à-vis asymptotics predictions : A beginning study

E.S. Nani ^{a,*}, Johannes Hötzer ^a, Britta Nestler ^{a,b}

^a Institute of Applied Materials (IAM-CMS), Karlsruhe Institute of Technology (KIT), Strasse am Forum 7, 76131 Karlsruhe, Germany

^b Institute of Digital Materials Science (IDM), Karlsruhe University of Applied Sciences, Moltkestrasse 30, 76133 Karlsruhe, Germany

ARTICLE INFO

Keywords:

Quantitative phase-field models

Large-interface artefacts

Interface-width reduction studies

Triple junctions

Young's law

Junction pinning

ABSTRACT

An ideal situation in phase-field methodology is when realistic evolution dynamics can be simulated at much larger interface widths. Asymptotic analysis, at best, can only help half address the challenge. It might give insights for making model adjustments so as to capture the appropriate sharp-interface description up to various orders of accuracy. However, this still is insufficient to conclude if artificial enlargement of interfacial thickness to desirable degree is permissible. Laborious numerical tests and crosschecks have to be performed to find it out. The current work will emerge to stand as a classic example for such a scenario. It is seen that sensitivity to modeling choices is more pronounced in the case of evolution of junctions than it is anywhere else. In particular, we noticed that interfacial mobility interpolating forms or formulations can put up severe restrictions on the required interface widths for reproducing close to converged sharp-interface behaviors. To make things worse, this is highly system dependent, i.e., the same material system considered in a different setup, or the same setup when considered for different material systems can require a change in mobility formulation for faster recovery of the limiting dynamics. Also, it is found that the traditional recipe popularly adopted for carrying out interface-width reduction studies is unsustainable and has to be replaced by a costlier routine.

1. Introduction

Phase-field methodology is the order of the day for simulating evolution dynamics in heterogeneous systems. It supplanted the sharp-interface treatments by facilitating an easier numerical integration of the involving governing equations. However, having been experimentally verified most of the time, the dynamical laws making up the sharp-interface problems are often considered more principal, and the diffuse-interface models are expected to recover them. The most direct way for establishing the success is by a formal analytical route called asymptotic analysis [1–3].

The routine of matched asymptotic analysis has been successfully executed for many phase-field models. Retrieval of the correct laws has also been demonstrated in majority of those cases. However, such a determination for any model is insufficient to conclude that the corresponding evolution dynamics will be readily reproduced when simulations are performed with it. The restrictiveness with regard to the amount of diffuseness of the interphase regions can potentially render the model impractical, except for studying certain qualitative behaviors. Therefore, besides establishing the limiting problem, the ease or lack thereof of its numerical realization has also to be determined, and possible ways of improving the convergence have to be suggested.

Such an exercise has been famously executed to completion in the case of dendritic solidification [4–11]. Other problems which boast the same status have invariably been the ones in which the phase-indicator variables are scalar valued—there have not been very many asymptotic analyses of multi-phase-field models. Among those available, the first of its kind is by Bronsard and Reitich [12], and the only other is its close adaptation by Wheeler et al. [13]. The former is for a simple isotropic grain-growth model, while Wheeler et al. extended it by the consideration of an additional concentration field. However, both the works confined to the case where the number of meeting phases is the bare minimum: three. That is, only triple junctions are analyzed for their asymptotic behavior but not the higher-order ones like quadruple junctions etc. This has recently been remedied by the current authors [14,15], while also verifying the asymptotics' predictions for binary interfaces [14]. The junctions' part remains to be tested, starting which is the objective of the current article.

The local/inner analysis of junction neighborhoods [15] predicted a rather surprising result. Namely that no matter what the interfacial energies, the bulk energies, the interfacial mobilities, and the interpolating forms that are chosen for the latter two are, the angles recovered

* Corresponding author.

E-mail address: sumanth.enugala@kit.edu (E.S. Nani).

at the junctions will always be as per the force balance calculation. For three meeting phases, this means the validity of Young's law irrespective of its state of motion [12,15]. The reason this is surprising is that closer models have reported a definite presence of an effect of interfacial mobilities or their interpolating forms on the simulated dihedral angles for moving triple junctions.

Particularly, Supriyo et al. [16] found that a grain couple solidifies with different angularities of the transformation front at the junction point, depending on what value is chosen for the solid–solid mobility. For the same grain setup but for growth from solutions, Wendler et al. [17] and Prajapati et al. [18] found that when an arithmetic form is chosen for the interpolation of the inverse mobilities, an elevation of the couple's value above that of the free surface's leads to a pinning effect at the tri-junction. This is in complete contradiction to the asymptotics predicted behavior. Granted, these models are not identical to the one for which asymptotic analysis has been explicitly carried out in Refs. [14,15], however, their phase-indicator parts are all almost the same. Therefore, with high chance, the conclusion still holds. The only possible reconciliation is that the observed deviation from the Young's law in the cases of Ref. [16] or Refs. [17,18] is a large interface artefact. It is worthwhile to carry out numerical tests to verify this proposition.

Here, we do the same for the isotropic grain-growth model considered in Refs. [14,15]. In particular, we ask: Does this model also show an influence of mobility function on the triple junction angles? If so, can it be explained in terms of the largeness of the interfacial width parameter ϵ ? Can a better mobility function be formulated such that simulations can be performed with large interfaces while still remaining close to the asymptotic limit behavior and thus reduce costs? What is the best mobility formulation which is the least restrictive with regard to the interface width irrespective of the material and topological properties of the microstructures? These questions will be under focus for much of the rest of the article. Apart from the obvious facilitation of cost-effective quantitative simulations, such an extensive characterization of the models and the modeling related choices is indispensable for setting up robust handles for their future manipulation and generalization to suit particular needs or applications.

First, some preparatory three grain evolution simulations are presented in the immediate next section. Following that, in Section 3, a commonly used prescription for conducting interface width reduction studies is shown to be ineffective, and a solution is proposed. Section 4 compares the relative merits of three different mobility interpolation formulations by conducting triple junction evolution studies for various grid discretizations and interface widths. Section 5 concludes the article.

2. Preparatory numerical simulations

2.1. Three-grain evolution in 2D

The simple grain-growth phase-field modeling equation studied in Refs. [14,15] is the following:

$$\tau(\phi) \frac{\partial \phi_\beta}{\partial t} = -\frac{1}{\epsilon} f_\alpha \frac{\partial g_\alpha(\phi)}{\partial \phi_\beta} - \frac{1}{\epsilon^2} \gamma \frac{\partial W(\phi)}{\partial \phi_\beta} + \gamma \nabla^2 \phi_\beta - \lambda, \quad \beta \in \{1, 2, \dots, N\}. \quad (1)$$

The various terms appearing in the above governing equation are given a detailed explanation multiple times in Refs. [14,15], and hence are not repeated here. The reader is urged to refer to the cited articles for the same. The asymptotic analysis of Eq. (1) has been successfully performed, and the prediction is that irrespective of what (but permissible) $\tau(\phi)$ is, Young's law has to be valid for a triple junction.

Eq. (1) is numerically solved for $N = 3$ for an initial setup depicted in Fig. 1. The choice of the interpolating forms and the multi-well form, and the selection of various material and simulation parameters are as

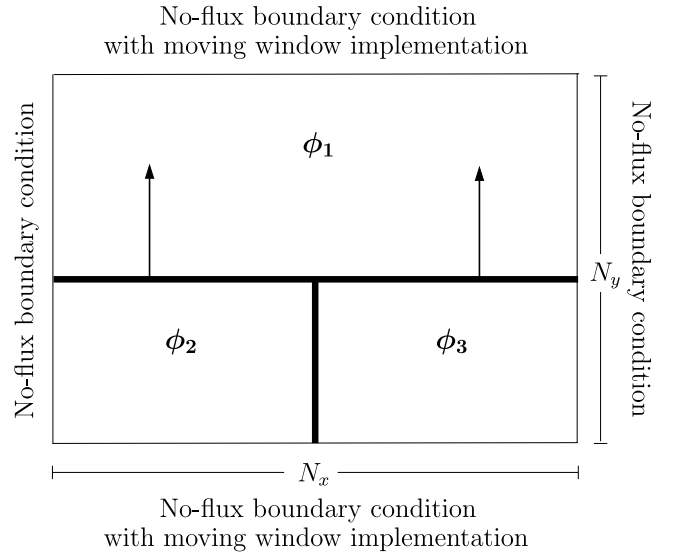


Fig. 1. A simulation setup used for the study of three phase growth. The growth direction is as depicted by the arrows and accordingly is the implementation of the shifting window.

Table 1

Table showing a parameter set used in the study of three phase growth within the setup of Fig. 1. N_x and N_y are the number of grid points in the x and y directions, respectively.

f_1	f_2	f_3	γ	τ_{12}	τ_{13}	N_x	N_y	Δx	Δt	ϵ
0.2	0.0	0.0	1.0	1.0	1.0	128	128	0.25	0.0125	1.25
$\{g_\alpha(\phi)\}$				$W(\phi)$				$\tau(\phi)$		
$\{\phi_\alpha^3(10 - 15\phi_\alpha + 6\phi_\alpha^2)\}$				$W^{FP} = 18[\phi_1^2(1 - \phi_1)^2 + \phi_2^2(1 - \phi_2)^2 + \phi_3^2(1 - \phi_3)^2]$				$\tau_\lambda = \frac{\sum_{\alpha < \beta} \tau_{\alpha\beta} \phi_\alpha^2 \phi_\beta^2}{\sum_{\alpha < \beta} \phi_\alpha^2 \phi_\beta^2}$		

listed in Table 1. The chosen values are such that phases ϕ_2 and ϕ_3 are interchangeable and grow at the expense of ϕ_1 . Thus, a moving window technique is implemented in the growth direction as indicated in the figure. The simulated steady-state profile shapes of the growth front for various values of τ_{23} are reported in Fig. 2. The corresponding steady-state speeds are tabulated in Table 2 along with the acute angles made by the fronts with the horizontal at the junction point. The solution of the sharp interface version of the steady-state problem,¹ with triple junction angles chosen in accordance with the Young's law, is also included in the figure and the table. Clearly, a considerable effect of the mobilities on the growth morphologies, including on the trijunction angles, can be seen, in seeming contrast to the predictions of the asymptotic analysis of Ref. [15].

In actual fact, there is no real contradiction here as the asymptotic analysis reveals only the vanishing interface-width limit behavior of the system. Hence, the laws it predicts need only be valid as ϵ tends to zero, and before that, different behaviors are indeed possible. Therefore, in the currently considered example, it might well be the case that the chosen value of $\epsilon = 1.25$ is not sufficiently small, especially more so for $\tau = 1000$ than $\tau = 1$ (i.e., larger values of inverse mobility than smaller ones), and on reducing it, the angles and the steady-state speeds may perhaps converge to the analytically predicted values tabulated in the bottom most row of Table 2. Nothing can be conclusively confirmed otherwise, and hence, we devote our attention to performing these tests. However, 'how small is small enough?' is a question that still needs to be addressed, which is a very non-trivial and difficult one to answer analytically. Hence, typically, numerical results are generated

¹ The problem statement and the solution steps are presented in Appendix.

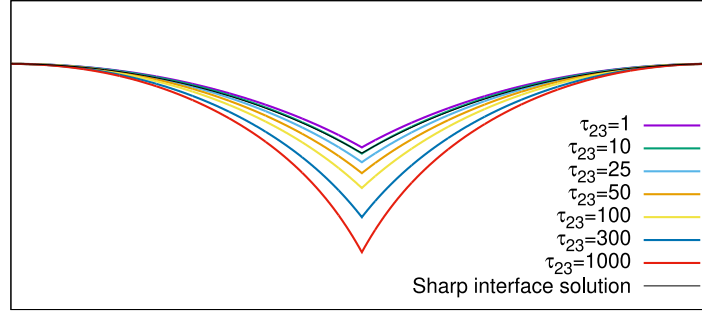


Fig. 2. Steady-state growth fronts realized in the simulations performed with the parameter set of Table 1 within the setup of Fig. 1 for various values of τ_{23} . Also depicted is the sharp interface theory predicted profile in black.

Table 2

Steady-state growth speeds realized in the simulations performed with the parameter set of Table 1 within the setup of Fig. 1 for various values of τ_{23} . Also listed is the sharp interface theory predicted growth speed.

τ_{23}	Recovered angle at the triple junction	Recovered steady-state speed (rel. error)
1	29.55724°	0.069110327 (3.50%)
10	31.81860°	0.067431019 (5.84%)
25	34.76556°	0.065186275 (8.98%)
50	38.60122°	0.062458562 (12.79%)
100	42.97858°	0.058963272 (17.67%)
300	52.02093°	0.052690495 (26.43%)
1000	61.14056°	0.045133604 (36.98%)
Sharp interface solution	30.0°	0.071616518

for progressively decreasing values of ϵ , and that value at which a further drop in the magnitude results only in a marginal change in the produced results is finalized to be a good enough choice, and the subsequent simulation studies are all performed with it. While this procedure may seem straightforward, it requires taking additional care for its proper execution:

Explicit finite difference schemes are commonly employed to solve the p.d.e.s arising in the phase-field approaches. In an attempt to simulate low interface widths, if the spatial discretization Δx is fixed and ϵ alone is reduced, the number of points corresponding to the interface keeps on decreasing, eventually leading to too few a points to sufficiently resolve it. Thus, one is forced to choose a rule connecting the two. Traditionally, ϵ is chosen proportional to the spatial discretization Δx . This demands that in order to simulate the same physical size of the system and yet decrease the interface width, the grid has to be necessarily made finer. Hence, the computational costs increase as some power of the grid fineness. More elaborately, if a particular discretization length is chosen to begin with, reducing it to half the original value is the same as doubling the fineness of the grid. Hence, the fineness factor is 2, and the number of grid points required to discretize the physical system increases as 2^d where d is the dimension of the domain. As a result, the number of calculations in each time step increase by the same amount. Moreover, the explicit finite difference scheme requires that when the grid spacing is decreased by a factor, due to the Laplacian nature of the Allen–Cahn equation, the timestep be reduced by the square of the factor for numerical stability. Therefore, to simulate the same physical size and the same physical time at half the interface width, a total of 2^{d+2} times more computational effort has to be expended.

Quite interestingly, numerical simulations revealed that even this costlier procedure is incapable of fetching the vanishing interface-width limiting behavior. This will be elucidated now.

Table 3

Effect of reducing the interface width by choosing ϵ proportional to Δx on the simulated growth speeds for three different proportionality constants. The expected speed is 0.1 units.

Δx	Fineness factor of the grid	Steady-state speed recovered with		
		$\epsilon = 4.0 \times \Delta x$	$\epsilon = 5.0 \times \Delta x$	$\epsilon = 6.0 \times \Delta x$
0.5 (base case)	1	0.090516	0.095858	0.097215
0.5/2	2	0.083321	0.095855	0.097278
0.5/4	4	0.043899	0.095673	0.097293
0.5/8	8	0	0.094919	0.097294
0.5/16	16	0	0.091821	0.097279
0.5/32	32	0	0.078190	0.097217
0.5/64	64	0	0	0.096969
0.5/128	128	0	0	0.095973
0.5/256	256	0	0	0.091879
0.5/512	512	0	0	0.073252
0.5/1024	1024	0	0	0

2.2. Two-phase evolution in 1D

The scalar version of Eq. (1) is the standard Allen–Cahn equation with driving force term:

$$\tau \frac{\partial \phi}{\partial t} = \frac{1}{\epsilon} \Delta f g'(\phi) - \gamma \frac{1}{\epsilon^2} f'_{\text{dw}}(\phi) + \gamma \nabla^2 \phi. \quad (2)$$

This equation is solved to simulate the evolution of a two phase 1D system starting from an initial setup of the left half of the domain filled with $\phi = 1$ and the right one with $\phi = 0$. The forms of the double well and the interpolation functions are chosen as $f_{\text{dw}}(\phi) = 18\phi^2(1 - \phi^2)$ and $g(\phi) = \phi^3(10 - 15\phi + 6\phi^2)$, respectively. The interfacial energy γ , bulk driving force Δf , and the mobility τ are selected as 1.0, 0.1 and 1.0, respectively. As a result, as per the predictions of the asymptotic analysis, the interface should move with a speed of $v^{(0)} = 0.1$ when it reaches the steady state. As no physics pertaining to a transport process governs the system dynamics, we fixed the number of grid cells at 10000 cells for running the simulations. The results obtained for various grid finenesses and proportionality constants are reported in Table 3. At the base fineness, the simulated speed is correct up to a value of a tenth of the calculated speed when ϵ is varied as four times Δx (first row, third column). As the fineness is increased, instead of tending towards the correct value, the simulated results diverged away from it eventually leading to a stagnant but diffuse interface. At higher proportionality constants, the behavior is delayed but remained fundamentally the same, as can be witnessed from columns 4 and 5 of the table. Thus, the ϵ proportional to Δx prescription proved to be ineffective in carrying out the interface width reduction investigations.

In the next section, an explanation is provided for this behavior. An efficacious prescription for realizing the vanishing ϵ limit in explicit finite difference schemes is also put forth. With it at disposal, the rest of the article will be dedicated for examining the speed of convergence of the simulations towards the asymptotic behavior predicted in Ref. [15]. Along the way, alternate choices of multi-well and interpolating forms

are considered from the point of view of reducing the computational costs.

However, before we move on, we establish a terminology which will be frequently employed through out the rest of the article: In the rest of the article, whenever the grid resolution or fineness is said to be varied, it is for the purposes of changing the interface width. Hence, no distinction is made between the two. That is, from here on, by simulations performed at higher (lower) resolutions or fineness factors, we mean the ones carried out at lower (higher) interface-widths or values of ϵ . The exact amount by which ϵ is reduced (increased) is either explicitly specified at appropriate places, or is made sure that it is clear from the context.

3. Efficacious ϵ v.s. Δx prescription for numerical realization of asymptotic limits

Let us consider the following governing equation, the one dimensional version of Eq. (2):

$$\tau \frac{\partial \phi}{\partial t} = \frac{1}{\epsilon} \Delta f g'(\phi) - \gamma \frac{1}{\epsilon^2} f'_{\text{dw}}(\phi) + \gamma \frac{\partial^2 \phi}{\partial x^2}. \quad (3)$$

The derivatives $\frac{\partial \phi}{\partial t}$ and $\frac{\partial^2 \phi}{\partial x^2}$ for any spatial point x and time t can be related to $\phi(x, t + \Delta t)$, $\phi(x - \Delta x, t)$, $\phi(x, t)$ and $\phi(x + \Delta x, t)$ using the Taylor's Remainder Theorem as

$$\frac{\partial \phi}{\partial t} \Big|_{(x,t)} = \frac{\phi(x, t + \Delta t) - \phi(x, t)}{\Delta t} - \frac{\Delta t}{2} \frac{\partial^2 \phi}{\partial t^2} \Big|_{(x,t^*)} \quad \text{for some } t^* \in (t, t + \Delta t) \quad \text{and}$$

$$\frac{\partial^2 \phi}{\partial x^2} \Big|_{(x,t)} = \frac{\phi(x + \Delta x, t) - 2\phi(x, t) + \phi(x - \Delta x, t)}{(\Delta x)^2} - \frac{(\Delta x)^2}{12} \frac{\partial^4 \phi}{\partial x^4} \Big|_{(x^*,t)} \quad \text{for some } x^* \in (x - \Delta x, x + \Delta x).$$

Therefore, Eq. (3), corresponding to the point (x, t) , can be re-expressed as

$$\tau \frac{\phi(x, t + \Delta t) - \phi(x, t)}{\Delta t} = \frac{\Delta f}{\epsilon} g'(\phi(x, t)) - \frac{\gamma}{\epsilon^2} f'_{\text{dw}}(\phi(x, t)) + \gamma \frac{\phi(x + \Delta x, t) - 2\phi(x, t) + \phi(x - \Delta x, t)}{(\Delta x)^2} + \underbrace{\tau \frac{\Delta t}{2} \frac{\partial^2 \phi}{\partial t^2} \Big|_{(x,t^*)} - \gamma \frac{(\Delta x)^2}{12} \frac{\partial^4 \phi}{\partial x^4} \Big|_{(x^*,t)}}_{\text{negligible}}. \quad (4)$$

However, in finite difference scheme, the above equation neglecting the last two terms is used for evaluating the phase-field value of the next time instant $t + \Delta t$ from the information pertaining to the current time t . That means, the implicit assumption is that the under-braced part of Eq. (4) is negligible compared to the rest of the equation. Invoking a stronger version of this, we assume that each of the terms of the under-braced part of Eq. (4) is minute when compared to each of the remaining terms of the equation. That is,

$$\begin{aligned} \tau \Delta t \left| \frac{\partial^2 \phi}{\partial t^2} \Big|_{(x,t^*)} \right| &\ll \tau \left| \frac{\phi(x, t + \Delta t) - \phi(x, t)}{\Delta t} \right| = \tau \left| \frac{\partial \phi}{\partial t} \Big|_{(x,t^*)} \right|, \\ \tau \Delta t \left| \frac{\partial^2 \phi}{\partial t^2} \Big|_{(x,t^*)} \right| &\ll \frac{1}{\epsilon} |\Delta f g'(\phi(x, t))|, \\ \tau \Delta t \left| \frac{\partial^2 \phi}{\partial t^2} \Big|_{(x,t^*)} \right| &\ll \frac{\gamma}{\epsilon^2} |f'_{\text{dw}}(\phi(x, t))|, \quad \text{and} \\ \tau \Delta t \left| \frac{\partial^2 \phi}{\partial t^2} \Big|_{(x,t^*)} \right| &\ll \gamma \left| \frac{\phi(x + \Delta x, t) - 2\phi(x, t) + \phi(x - \Delta x, t)}{(\Delta x)^2} \right| = \gamma \left| \frac{\partial^2 \phi}{\partial x^2} \Big|_{(x^*,t)} \right| \end{aligned}$$

for some $t^* \in (t, t + \Delta t)$ and $x^* \in (x - \Delta x, x + \Delta x)$. Similarly,

$$\gamma (\Delta x)^2 \left| \frac{\partial^4 \phi}{\partial x^4} \Big|_{(x^*,t)} \right| \ll \tau \left| \frac{\partial \phi}{\partial t} \Big|_{(x,t^*)} \right|,$$

$$\gamma (\Delta x)^2 \left| \frac{\partial^4 \phi}{\partial x^4} \Big|_{(x^*,t)} \right| \ll \frac{1}{\epsilon} |\Delta f g'(\phi(x, t))|,$$

$$\gamma (\Delta x)^2 \left| \frac{\partial^4 \phi}{\partial x^4} \Big|_{(x^*,t)} \right| \ll \frac{\gamma}{\epsilon^2} |f'_{\text{dw}}(\phi(x, t))|, \quad \text{and}$$

$$\gamma (\Delta x)^2 \left| \frac{\partial^4 \phi}{\partial x^4} \Big|_{(x^*,t)} \right| \ll \gamma \left| \frac{\partial^2 \phi}{\partial x^2} \Big|_{(x^*,t)} \right|.$$

The actual solution of Eq. (3) is $\tanh((x - vt)/\epsilon)$ for the choice $f_{\text{dw}}(\phi) = 18\phi^2(1 - \phi^2)$ and $g(\phi) = \phi^3(10 - 15\phi + 6\phi^2)$, with v standing for $\Delta f/\tau$. Therefore, $\frac{\partial^2 \phi}{\partial t^2} \Big|_{(x,t^*)} = \mathcal{O}\left(\frac{1}{\epsilon^2}\right)$, $\frac{\partial \phi}{\partial t} \Big|_{(x,t^*)} = \mathcal{O}\left(\frac{1}{\epsilon}\right)$, $\frac{\partial^2 \phi}{\partial x^2} \Big|_{(x,t^*)} = \mathcal{O}\left(\frac{1}{\epsilon^2}\right)$, and $\frac{\partial^4 \phi}{\partial x^4} \Big|_{(x,t^*)} = \mathcal{O}\left(\frac{1}{\epsilon^4}\right)$. Hence, calculations pertaining to

the numerical scheme give small errors only when

$$\begin{aligned} \frac{\Delta t}{\epsilon^2} \ll \frac{1}{\epsilon} &\implies \Delta t \ll \epsilon & \frac{(\Delta x)^2}{\epsilon^4} \ll \frac{\Delta f}{\gamma \epsilon} &\implies (\Delta x)^2 \ll \frac{\Delta f}{\gamma} \epsilon^3 \\ \frac{\Delta t}{\epsilon^2} \ll \frac{1}{\epsilon^2} &\implies \Delta t \ll 1 & \frac{(\Delta x)^2}{\epsilon^4} \ll \frac{1}{\epsilon^2} &\implies (\Delta x)^2 \ll \epsilon^2. \end{aligned}$$

Furthermore, since explicit finite difference schemes are used for solving the evolution equation, for numerical stability, Δt has to be chosen such that $\Delta t \leq \frac{\tau(\Delta x)^2}{2d\gamma}$. Therefore, it suffices that the spatial

discretization and the interface width specifier satisfy

$$\begin{aligned} (\Delta x)^2 &\ll 1, \\ (\Delta x)^2 &\ll \epsilon, \\ (\Delta x)^2 &\ll \epsilon^2, \quad \text{and} \\ (\Delta x)^2 &\ll \frac{\Delta f}{\gamma} \epsilon^3. \end{aligned}$$

Of course, the above relations will necessarily hold true when Δx is brought close to zero keeping ϵ constant. However, if ϵ itself is made to tend to zero, then the relative vanishing rates should be carefully chosen so as to satisfy the relations. Specifically, in the limit $\epsilon \rightarrow 0$, the last relation is the significant one, since, once it is satisfied, the others are automatically follow. Let ϵ be chosen as a power of Δx , i.e., $\epsilon = k(\Delta x)^p$. The last condition then requires

$$(\Delta x)^{2-3p} \ll \frac{\Delta f}{\gamma} k^3. \quad (5)$$

As Δx is progressively reduced, Eq. (5) will necessarily be 'eventually satisfied' if and only if $2 - 3p > 0$. In other words, to approach the asymptotic limit of $\epsilon \rightarrow 0$ in numerics by implementing a finite difference explicit scheme, it has to be ensured that $(\Delta x)^{\frac{2}{3}} = o(\epsilon)$ as $\Delta x \rightarrow 0$. This explains the failure of the $\epsilon \propto \Delta x$ prescription observed in Table 3: When p is chosen as 1, Eq. (5) becomes

$$\frac{1}{\Delta x} \ll \frac{\Delta f}{\gamma} k^3. \quad (6)$$

For as long as Δx fulfills the above condition, the errors incurred in approximating the partial differential equation with the explicit finite difference equation are small, and hence the recovered dynamics is close to the actual behavior. However, as Δx is reduced progressively, it incrementally begins to violate the above requirement, and hence, results diverging away from the desired behavior are realized. Further, a value of Δx that fails to fulfill Eq. (6) for some prefactor k , does so by lesser amount for higher values of the latter. Consistent with this, the error in the predicted dynamics drops along each row in Table 3.

Eq. (6) also points out the effect that the driving force Δf and the interfacial energy γ are going to have on the range of allowable grid spacings. It is well known that a large value of the driving force removes points from the interface, and hence demands a larger value of the coefficient k for sustaining a stable simulation. On the other hand, it is usually believed that a low driving force does not pose any such difficulty. In contrast, Eq. (6) suggests that when the driving force

Table 4

Speeds recovered in simulations as interface width is reduced whilst choosing $\epsilon = 6.0 \times \Delta x$ for three different values of the driving force specifier Δf viz. 0.1, 0.01 and 0.001. The expected speeds are 0.1, 0.01 and 0.001, respectively. For the simulations of the last two columns, the number of grid cells considered are 2000.

Δx	Fineness factor	Simulated speed recovered for		
		$\Delta f = 0.1$	$\Delta f = 0.01$	$\Delta f = 0.001$
0.5 (base case)	1	0.097215	0.0097209	0.00096374
0.5/2	2	0.097278	0.0097287	0.00094050
0.5/4	4	0.097293	0.0097180	0.00083504
0.5/8	8	0.097294	0.0096794	0
0.5/16	16	0.097279	0.0095213	0
0.5/32	32	0.097217	0.0088681	0
0.5/64	64	0.096969	0.0055310	0
0.5/128	128	0.095973	0	0
0.5/256	256	0.091879	0	0
0.5/512	512	0.073252	0	0
0.5/1024	1024	0	0	0

Table 5

Simulated steady-state speeds as interface width is reduced by choosing $\epsilon = 4.0 \times \Delta x$ for various values of interfacial energy specifier γ . The expected speed is 0.1.

Δx	Fineness factor	Simulated speed recovered for		
		$\gamma = 1.0$	$\gamma = 0.25$	$\gamma = 0.0625$
0.5 (base case)	1	0.090516	0.091987	0.083559
0.5/2	2	0.083321	0.092053	0.090045
0.5/4	4	0.043899	0.090487	0.091959
0.5/8	8	0	0.083318	0.092065
0.5/16	16	0	0.043920	0.090484
0.5/32	32	0	0	0.083313
0.5/64	64	0	0	0.043932
0.5/128	128	0	0	0

Table 6

Study of [Table 3](#) repeated instead by choosing ϵ proportional to $\sqrt{\Delta x}$ for the same proportionality constants.

Δx	Fineness factor	Steady-state speed recovered with		
		$\epsilon = 4.0 \times \sqrt{\Delta x}$	$\epsilon = 5.0 \times \sqrt{\Delta x}$	$\epsilon = 6.0 \times \sqrt{\Delta x}$
0.5 (base case)	1	0.096740570	0.097990192	0.098572284
0.5/2	2	0.098488824	0.099034747	0.099306608
0.5/4	4	0.099269114	0.099526360	0.099657746
0.5/8	8	0.09963862	0.099764334	0.099829382
0.5/16	16	0.099819862	0.099882168	0.099914606
0.5/32	32	0.099910263	0.099941214	0.099957375
0.5/64	64	0.099955217	0.099970638	0.099978705
0.5/128	128	0.099977623	0.099985324	0.099989353
0.5/256	256	0.099988813	0.099992662	0.099994676
0.5/512	512	0.099994408	0.099996333	0.099997339
0.5/1024	1024	0.099997203	0.099998170	0.099998670

is too small, an otherwise effective grid spacing leads to undesirable magnitudes of error. This is demonstrated in [Table 4](#) which corresponds to the same simulations as the last column of [Table 3](#), but with smaller values of Δf viz. $\Delta f = 0.1$ and 0.01. The lower the driving force, the faster is the approach towards stagnation of the interface. The opposite effect of γ is illustrated in [Table 5](#). All these problems can be avoided by choosing $\epsilon > (\Delta x)^{\frac{2}{3}}$, this is demonstrated in [Tables 6, 7](#) and [8](#) where the results of the simulations corresponding to [Tables 3, 4](#) and [5](#) are re-performed but with ϵ chosen as $\epsilon = k\sqrt{\Delta x}$ consistent with Eq. (5). The contrasting behavior of the results converging towards the expected answer when the grid is made finer can be readily recognized.

To consolidate, for realizing the vanishing interface-width limit behavior of the derived phase-field model in explicit schemes, Δx should be made to vanish faster than ϵ . This implies that the number of grid points corresponding to the interfacial region keeps on scaling up as the interface width is reduced. That is, the numerical recovery of asymptotic limit is a far more expensive procedure than the estimates provided in Section 2.

Table 7

Study of [Table 4](#) re-performed instead with $\epsilon = 6.0 \times \sqrt{\Delta x}$.

Δx	Fineness factor	Simulated speed recovered for		
		$\Delta f = 0.1$	$\Delta f = 0.01$	$\Delta f = 0.001$
0.5 (base case)	1	0.098572284	0.009882372	0.000988252
0.5/2	2	0.099306608	0.009941124	0.000994115
0.5/4	4	0.099657746	0.009969976	0.000996997
0.5/8	8	0.099829382	0.009984056	0.000998406
0.5/16	16	0.099914606	0.009992258	0.000999226
0.5/32	32	0.099957375	0.009996080	0.000999608
0.5/64	64	0.099978705	0.009998048	0.000999805
0.5/128	128	0.099989353	0.009999024	0.000999902
0.5/256	256	0.099994676	0.009999511	0.000999951
0.5/512	512	0.099997339	0.009999756	0.000999976
0.5/1024	1024	0.099998670	0.009999878	0.000999987

Table 8

Study of [Table 5](#) re-performed instead with $\epsilon = 4.0 \times \sqrt{\Delta x}$.

Δx	Fineness factor	Speed recovered for		
		$\gamma = 1.0$	$\gamma = 0.25$	$\gamma = 0.0625$
0.5 (base case)	1	0.096740570	0.095743965	0.084264066
0.5/2	2	0.098488824	0.098060608	0.092243193
0.5/4	4	0.099269114	0.099064623	0.096129851
0.5/8	8	0.09963862	0.099540896	0.098062178
0.5/16	16	0.099819862	0.099771958	0.099028455
0.5/32	32	0.099910263	0.099886604	0.099513178
0.5/64	64	0.099955217	0.099943431	0.099756302
0.5/128	128	0.099977623	0.099971748	0.099878092
0.5/256	256	0.099988813	0.099985879	0.099939033
0.5/512	512	0.099994408	0.099992943	0.099969510
0.5/1024	1024	0.099997203	0.099996470	0.099984752

Before we move on, it must be pointed out that not all the aspects of the numerical analysis associated with the problem are taken into consideration for deriving the prescription of Eq. (5): For one, the errors incurred in marching, as per the chosen finite difference scheme, from time t to $t + \Delta t$ are evaluated under the assumption that the exact solution corresponding to the former time instant is available. Whereas, in actuality, the available information pertaining to time t is also approximate, itself being obtained in the same fashion in the preceding timestep. That is, the ‘‘instantaneous’’ errors are calculated without taking into account their propagation along the way. Secondly, a second set of calculations pertaining to passage to a global analysis from the local one considered herein has to be ideally carried out which puts further constraints on the allowable ranges of discretization. This is elucidated by considering the following example, the classical diffusion equation:

$$\frac{\partial c}{\partial t} = D\nabla^2 c.$$

Repeating the calculations of the current section for this equation merely demands that Δt and Δx have to be kept vanishingly small for controlling the errors. That is, only $\Delta t \ll 1$ and $\Delta x \ll 1$ is demanded, but not any further condition concerning their relative orders. However, it is well known that only when Δt is varied as $\Delta t \leq (\Delta x)^2/2dD$, the explicit finite difference scheme will be stable. The equations corresponding to all the grid points have to be simultaneously considered and analyzed for obtaining this result. Such a second layer of analysis is not performed on the entirety of Eq. (3), and is not even possible to do due to its non-linear nature. In spite of this, it became possible to explain the behaviors of [Tables 3, 4](#) and [5](#), and rectify them to [Tables 6, 7](#), and [8](#), respectively. Not only that, as will be witnessed next, the relation Eq. (5) proves to be efficacious in all the 2D problems and even those involving triple junctions, i.e., even for multi-phase-field applications, notwithstanding the fact that it is derived merely by considering a very specific scalar 1D modeling equation. Seeing that so many details are left out, it has to be considered a happy accident that the part that could actually be done was of such immense help in setting

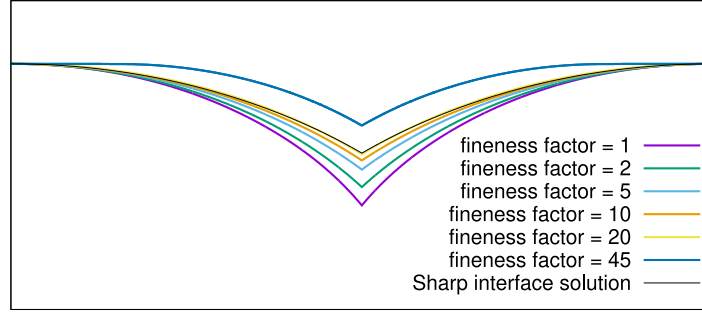


Fig. 3. The $\tau_{23} = 100$ case of Fig. 2 re-studied at various degrees of grid fineness using Toth's multi-well $W^T = 36 \left(\frac{\phi_1^4 + \phi_2^4 + \phi_3^4}{4} + \frac{\phi_1^2 \phi_2^2 + \phi_2^2 \phi_3^2 + \phi_3^2 \phi_1^2}{2} - \frac{\phi_1^3 + \phi_2^3 + \phi_3^3}{3} - \frac{1}{12} \right)$ and by turning off the Lagrange multiplier implementation. The prescription of $\epsilon = 5.0 \times \Delta x$ is utilized for the simulations with the resolution of Table 1 corresponding to fineness factor = 2.

Table 9

Steady-state angles and speeds recovered for the growth fronts of Fig. 3.

Fineness factor	Simulated angle at the triple junction	Simulated steady-state speed (rel. error)
1	50.26812°	0.055692812 (22.23%)
2	42.65556°	0.059691085 (16.65%)
5	36.56480°	0.063862144 (10.83%)
10	33.52546°	0.066000236 (7.84%)
20	31.78469°	0.067073856 (6.34%)
40	30.26082°	0.062963142 (12.08%)
Sharp interface solution	30.0°	0.071616518

straight the prescription for approaching the vanishing interface-width limit in numerics.

The numerical performance of the multi-phase-field governing equations will be considered next.

4. Triple junction behavior in numerical simulations

The asymptotics predicted limiting dynamics of binary interfaces governed by Eq. (1) has been verified in Ref. [14]. We now focus on the numerical realization of the asymptotic laws predicted for the triple junction dynamics. Particularly, we look at the recovery of the Young's law.

Two things can be conjectured from the discussion thus far: First, the influence of the mobilities on the triple junction angles in the motivating example presented at the beginning of Section 2 could possibly be a large interface artefact. And the second, the $\epsilon \propto \Delta x$ might not be an effective prescription for checking this. It will now be demonstrated that these impressions are indeed true.

The $\tau_{23} = 100$ case of Fig. 2 is re-performed for various grid finenesses but by choosing Toth's well $W^T = 36 \left(\frac{\phi_1^4 + \phi_2^4 + \phi_3^4}{4} + \frac{\phi_1^2 \phi_2^2 + \phi_2^2 \phi_3^2 + \phi_3^2 \phi_1^2}{2} - \frac{\phi_1^3 + \phi_2^3 + \phi_3^3}{3} - \frac{1}{12} \right)$ and switching off the Lagrange multiplier implementation. This combination minimizes the occurrence of third phases inside the binary interfaces [14]. The relation between ϵ and the grid spacing Δx is varied as $\epsilon = 5.0 \times \Delta x$. The results are reported in Fig. 3 and Table 9. As the interface width is reduced, the profiles are seen to incrementally improve until a resolution of 20 \times , after which they suddenly behave in an eccentric manner. The abnormal behavior is suspected to be emerging from the inefficacy of the ϵ proportional to Δx selection. However, it is not feasible to test this for the current parameter set as it would require going up to over 900 times higher resolution when using $\epsilon = 5.0 \sqrt{\Delta x}$.

Therefore, a different parameter set is constructed exclusively for testing this hypothesis. The analysis of Section 3 proposes that the $\epsilon \propto \Delta x$ scheme fails faster at lower driving forces. Thus, by reducing the

Table 10

A parameter set designed to prove that the jump behavior of Fig. 3 is due to the $\epsilon \propto \Delta x$ selection.

f_1	f_2	f_3	γ	τ_{12}	τ_{13}	τ_{23}	N_x	N_y	Δx	Δt	
0.50	0.0	0.0	1.0	1.0	1.0	1.0	64	32	1.0	$0.2 \times (\Delta x)^2$	
$\{g_\alpha(\phi)\}$				$W(\phi)$				$\tau(\phi)$			
$\{\phi_\alpha^3(10 - 15\phi_\alpha + 6\phi_\alpha^2)\}$				$W^T(\phi)$ with $a = 36$				$\tau_A(\phi)$			

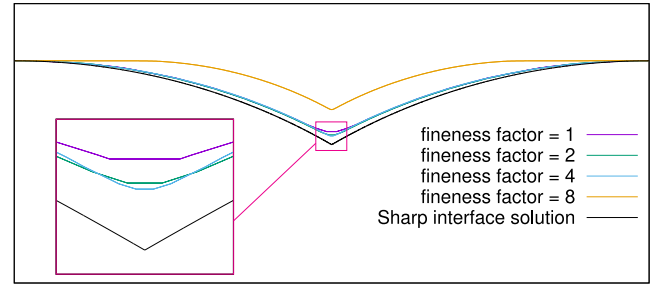


Fig. 4. Simulation results at various degrees of fineness of the grid obtained by varying ϵ as $\epsilon = 4.5 \times \Delta x$. The values of Table 10 are chosen for the base resolution.

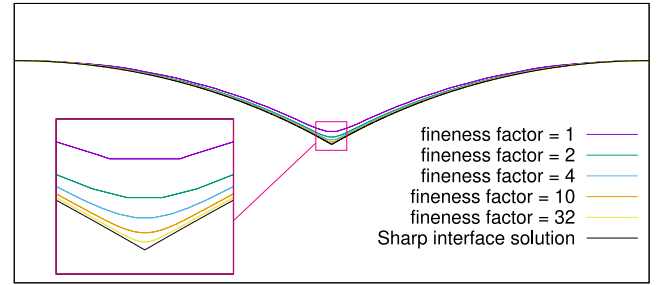


Fig. 5. Simulation results at various degrees of fineness of the grid obtained by varying ϵ as $\epsilon = 4.5 \times (\Delta x)^{0.6}$. The values of Table 10 correspond to the base resolution.

latter, this hypothesis may be tested. However, when the bulk driving force is too small, one may run into the problem of the solid phases shrinking rather than growing due to their curvatures. Thus, to control the curvatures, larger lengths in the lateral direction are chosen and a parameter set is designed which is listed in Table 10. The associated simulation results are reported in Figs. 4 and 5, and in Table 11.

In the $\epsilon = 4.5 \times \Delta x$ simulations, after a fineness of 8 \times , the front motion stopped abruptly whereas when $\epsilon = 4.5 \times (\Delta x)^{0.6}$, at 40 \times , that is, at even smaller interface widths, the profile behaved in a fashion that is normal. Thus, it can be concluded that the sudden change in the profile

Table 11
Steady-state speeds recovered for the growth fronts of (a) Fig. 4 and (b) Fig. 5.

(a)		(b)	
Fineness of the grid	Speed recovered with $\epsilon = 4.5 \times \Delta x$	Fineness of the grid	Speed recovered with $\epsilon = 4.5 \times (\Delta x)^{0.6}$
1	0.009057744	1	0.009057744
2	0.009172148	2	0.009493199
4	0.009012258	4	0.009644454
6	0.008199712	6	0.009697528
7	0.006742424	8	0.009722445
8	-2.025757E-13	10	0.009736554
Sharp interface solution	0.009790374	20	0.009765793
		32	0.009776316
		40	0.009779809

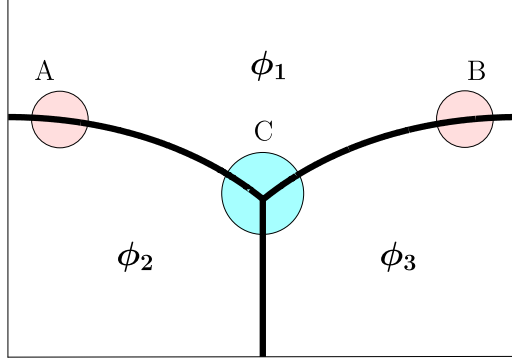


Fig. 6. Schematic of the steady-state profile of the three grain growth within the setup of Fig. 1, with triple junction region and regions well removed from it highlighted.

shape in Fig. 3 is an outcome of the restrictive choice of the relation between interface width and spatial discretization.

4.1. Explanation of the slow convergence in Fig. 3

We will now try to reason why the case of Fig. 3 required such high resolutions to come close to realizing the limiting behavior, whereas that of Fig. 4 did not. First of all, we will dispose of the possibility of a role played by binary interfaces. In Ref. [14], a third phase with very low mobility materialized inside a binary interface as a first-order error that scaled with the interface width. This retarded the motion and thus delayed the convergence. Such a thing, however, cannot happen in the current case: the usage of Toth potential and the choice of leaving out Lagrange multiplier implementation ensures that the binary interfaces are free from the third phases up to the first order [14]. That means, whatever interplay may be responsible for the sluggish convergence must only be limited to the triple junction neighborhoods and not to regions farther away. In particular, the reason has to do with the specific choice of the inverse mobility function $\tau(\phi)$, as $\tau_A(\phi)$ of Table 1, which regulates the junction mobility in a characteristic manner.

Consider the schematic of Fig. 6, and let us assume that the simulation parameter set is as given in Table 1, except maybe for a replacement of W^{FP} with W^T . The regions marked A and B which are well removed from the triple point see a bulk driving force of 0.1, and an inverse mobility of 1.0, due to the $\tau_A(\phi)$ merging into τ_{12} and τ_{13} , respectively, at zeroth order. Whereas, the region marked C has the values of all the phase-field components around $1/3$, and as a rough estimate, sees an inverse mobility of $\frac{1 \times 1/3 \times 1/3 + 1 \times 1/3 \times 1/3 + 100 \times 1/3 \times 1/3}{1/3 \times 1/3 + 1/3 \times 1/3 + 1/3 \times 1/3} = 34$,

and possibly not a strikingly different overall driving force. Hence, the region C has almost the same propensity to grow but its mobility is much lower compared to regions A and B, and hence, the interface gets pinned to some extent at the triple junction. Furthermore, as ϵ is reduced, the percentage of the front region that is associated with

Table 12
Steady-state angles and speeds recovered for the growth fronts of Fig. 7.

Fineness factor	Simulated angle at the triple junction	Simulated steady-state speed (rel. error)
1	35.78360°	0.067906155 (5.18%)
2	29.75446°	0.068478003 (4.38%)
5	29.48043°	0.068868911 (3.84%)
10	29.43619°	0.068930519 (3.75%)
20	29.63458°	0.068655565 (4.13%)
40	29.19031°	0.063279723 (11.64%)
Sharp interface solution	30.0°	0.071616518

Table 13
Steady-state angles and speeds recovered for the growth fronts of Fig. 8.

Fineness factor	Simulated angle at the triple junction	Simulated steady-state speed (rel. error)
1	35.44136°	0.068944773 (3.73%)
2	32.10509°	0.069987781 (2.27%)
5	30.68639°	0.070741189 (1.22%)
10	30.39941°	0.071060387 (0.78%)
20	30.25262°	0.071261178 (0.50%)
40	30.15823°	0.071388989 (0.32%)
Sharp interface solution	30.0°	0.071616518

low mobility reduces, and thereby the pinning is relieved. Eventually, in the sharpest of the interface widths, only the triple point, i.e., a set of measure zero sees a different value, and hence the pinning effect is completely eliminated. This also explains the faster convergence in the case pertaining to Fig. 4. In it, the inverse mobilities of all the three interfaces are chosen to be of the same magnitude of 1, and hence, the value resulted for the junction is also 1. Therefore, it did not matter how much of the front region corresponded to the junction neighborhood, as all of the regions have the same mobility.

In summary, the slow convergence in Fig. 3 is an outgrowth of the inverse mobility interpolating form. Therefore, to realize convergence without having to adopt the costly approach of ϵ reduction, a different interpolation form for $\tau(\phi)$ may be chosen.

4.2. Alternate interface mobility formulations

4.2.1. Harmonic form of τ interpolation

In particular, if $\tau(\phi)$ is averaged in a harmonic fashion, $\tau_H(\phi)$, given by

$$\frac{1}{\tau_H(\phi)} = \frac{\sum_{\alpha < \beta} \frac{1}{\tau_{\alpha\beta}} \phi_\alpha^2 \phi_\beta^2}{\sum_{\alpha < \beta} \phi_\alpha^2 \phi_\beta^2}, \quad (7)$$

as opposed to the arithmetic one, $\tau_A(\phi)$ of Table 1, the value seen at regions A and B is still unity, but the one seen at C is around 1.5 instead of 34. Therefore, the hinging of the triple junction can be drastically reduced.

Results of simulations performed at various resolutions but for the new τ -form are reported in Fig. 7 and Table 12. Note that the trijunction angle and speed of advancement of the surface recovered are very close to the theoretical values even at low resolutions. Once again, the abrupt behavior in the profile shape can be witnessed at large resolutions due to the ϵ proportional to Δx scheme of reducing the interface width. Simulations re-done instead by choosing $\epsilon \propto (\Delta x)^{0.6}$ eliminated this, as evident from Fig. 8 and Table 13. Not only that, the quality of convergence is also bettered: A slight gap between the sharp interface solution and the simulated profiles persisted in Fig. 7, even at values of grid fineness in the ideal range. Whereas, no such visible gap is seen in the case of $\epsilon = 5.0 \times (\Delta x)^{0.6}$. Furthermore, the growth speed is also seen to attain the steady-state value in a clean fashion in the

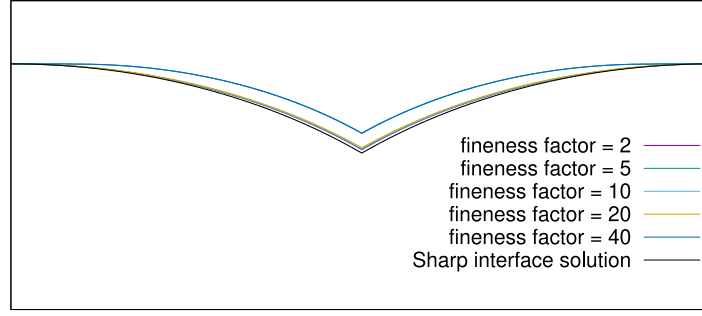


Fig. 7. Simulations of Fig. 3 re-performed with inverse mobility interpolation chosen in a harmonic fashion as in Eq. (7)..

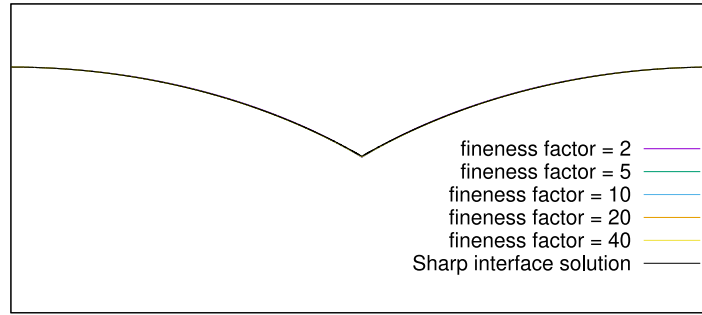


Fig. 8. Simulations of Fig. 7 re-performed by instead varying ϵ as $\epsilon = 5.0 \times (\Delta x)^{0.6}$.

latter case without an oscillatory behavior observed in the former (not reported).

Though the change in the form used for interpolating the mobilities solved the particular problem at hand, it is in no way an exhaustive solution. Arithmetic average of a set of numbers stays close to the largest of the values while the harmonic one to that of the smallest. Hence, in the current example, where it is advantageous to pick the smaller value, harmonic form proved to be the efficient one. However, in problems where the growth front of interest is itself less mobile, and a part of it is contributed from a triple junction that is highly mobile, then the opposite situation would result. That is, it would then be beneficial to pick a larger value instead of a smaller one, and hence the arithmetic form, in principle, will turn out to be the better among the two choices. Like how the arithmetic form led to the pinning of the triple junction in the current case, in such a situation, a protrusion of the junction is likely to take place, with the rest of the front lagging behind. However, simulations performed with the same parameter set as used for Fig. 8 except for a reversal of the inverse mobility values as $\tau_{12} = 100$, $\tau_{13} = 100$ and $\tau_{23} = 1$, did not produce any such protrusion, or, as a matter of fact, any huge differences in the computational results, as can be seen from the first two rows of Table 14 and from the second and third columns of Table 15. The arithmetic form is found to be only slightly better when compared to the harmonic one, both in terms of the front shapes and their growth speeds. Heightened differences can be seen at larger driving forces, as shown in Table 16. Where, for resolutions 1 and 2, the harmonic form gave rise to an oscillatory instability while the arithmetic one remained stable, and at resolution 4, the former exhibited a protrusion. However, as is typically the case, the interface widths required to retrieve results up to the same level of accuracy are smaller at higher driving forces. Hence, though better than the harmonic one, the arithmetic form itself behaved badly (i.e., convergence is very sluggish), as is evident from

the table. Strikingly, even though a huge difference is seen among the profile shapes, the recovered growth speeds deviated only slightly as revealed by Table 17.

It has to be acknowledged at this point that the arithmetic to harmonic switch was already suggested by Wendler et al. [17], and adopted by Prajapati et al. [18]. However, in those works, the deviation in the case of arithmetic or agreement in the case of harmonic are believed to be final behaviors. That is, they are not concluded as emerging from the sensitiveness or insensitiveness of the model+ setup combination with regard to the interface-width. We also mention that the current authors independently constructed the argument for why harmonic form is superior to arithmetic in the case of $\tau_{23} \gg \tau_{12} \approx \tau_{13}$ for the setup of Fig. 1.

4.2.2. Steinbach's τ -formulation

At this juncture, it may be interesting to consider a τ -formulation proposed by Steinbach [19] which does not involve any kind of averaging or interpolation. The governing equations in such a model read

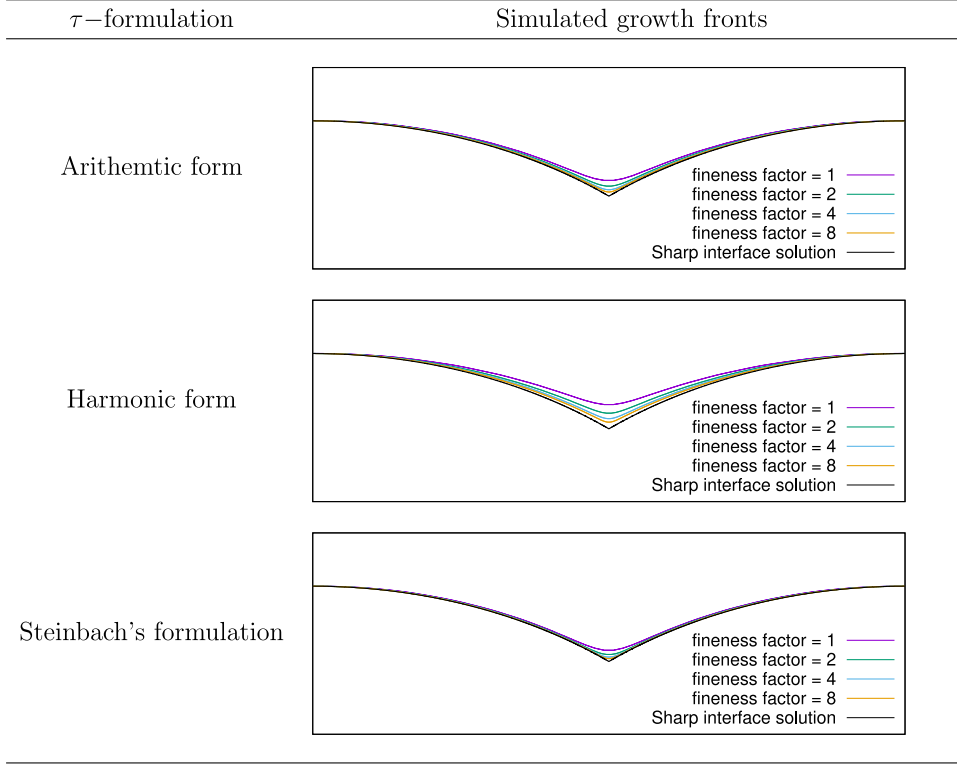
$$\frac{\partial \phi_\alpha}{\partial t} = -\frac{1}{N} \sum_{\beta \neq \alpha}^N \frac{1}{\tau_{\alpha\beta}} \left(\frac{\delta F}{\delta \phi_\alpha} - \frac{\delta F}{\delta \phi_\beta} \right) \quad \forall \alpha \in \{1, 2, \dots, N\} \quad (8)$$

where the variational derivatives have the standard form as those of Eq. (1). It has to be cautioned, however, that the bulk energy interpolating forms have to be necessarily chosen as $g_\alpha(\phi) = \phi_\alpha \forall \alpha \in \{1, 2, \dots, N\}$. It will now be shown that even with these equations, the binary interfaces being free of any other phases at the leading order, and the force balance requirement holding true at the junctions, are both recovered in the limit of $\epsilon \rightarrow 0$.

First of all, it is easy to recognize that the summation property is facilitated by the above equations. Next, in the local coordinates pertaining to a binary interface, the requirement at the leading order

Table 14

Simulations performed with the parameter set used for Fig. 8 but with three different mobility formulations and a modification of the inverse mobility values as $\tau_{12} = \tau_{13} = 100$ and $\tau_{23} = 1$. That is, the growth front is made less mobile and the mobility of the interface between the bottom two grains is enhanced.

**Table 15**

Steady-state angles and speeds recovered for the growth fronts of Table 14.

Fineness factor	Speed recovered with		
	Arithmetic form	Harmonic form	Steinbach's formulation
1	0.000710319	0.000744610	0.000921221
2	0.000714586	0.000735689	0.000934725
4	0.000716372	0.000729509	0.000941852
8	0.000716966	0.000725348	0.000945626
Sharp interface theory predicted speed			0.00071616518

is

$$\begin{bmatrix} 0 \\ 0 \\ \cdot \\ \cdot \\ \cdot \\ 0 \end{bmatrix} = \frac{1}{N} \begin{bmatrix} \frac{1}{\tau_{1*}} & -\frac{1}{\tau_{12}} & \cdots & -\frac{1}{\tau_{1N}} \\ -\frac{1}{\tau_{21}} & \frac{1}{\tau_{2*}} & \cdots & -\frac{1}{\tau_{2N}} \\ \cdot & \cdot & \cdots & \cdot \\ \cdot & \cdot & \cdots & \cdot \\ \cdot & \cdot & \cdots & \cdot \\ -\frac{1}{\tau_{N1}} & -\frac{1}{\tau_{N2}} & \cdots & \frac{1}{\tau_{N*}} \end{bmatrix} \begin{bmatrix} -\gamma \frac{\partial W(\phi)}{\partial \phi_1}(\tilde{\phi}^{(0)}) + \gamma \frac{\partial^2 \tilde{\phi}_1^{(0)}}{\partial \rho^2} \\ -\gamma \frac{\partial W(\phi)}{\partial \phi_2}(\tilde{\phi}^{(0)}) + \gamma \frac{\partial^2 \tilde{\phi}_2^{(0)}}{\partial \rho^2} \\ \cdot \\ \cdot \\ \cdot \\ -\gamma \frac{\partial W(\phi)}{\partial \phi_N}(\tilde{\phi}^{(0)}) + \gamma \frac{\partial^2 \tilde{\phi}_N^{(0)}}{\partial \rho^2} \end{bmatrix} \quad (9)$$

where $\tau_{\alpha\beta} = \tau_{\beta\alpha}$ as usual, and $\tau_{\alpha*}$ is given by

$$\frac{1}{\tau_{\alpha*}} = \sum_{\substack{\beta=1 \\ \beta \neq \alpha}}^N \frac{1}{\tau_{\alpha\beta}}.$$

It can be readily verified that a column matrix with all the entries being the same belongs to the null space of the above matrix $\left\{ \frac{1}{\tau_{\alpha\beta}} \right\}$. Furthermore, if it is assumed that they are the only kind of vectors that are present in the null space, the requirement for the leading order term

of the asymptotic expansion of the phase-field variable is

$$\gamma \frac{\partial^2 \tilde{\phi}_\alpha^{(0)}}{\partial \rho^2} - \gamma \frac{\partial W(\phi)}{\partial \phi_\alpha}(\tilde{\phi}^{(0)}) = f(\tilde{\phi}^{(0)}) \quad \forall \alpha \in \{1, 2, \dots, N\} \quad (10)$$

for some function $f(\tilde{\phi}^{(0)})$. Summing up all the equations, i.e., over all α , the function turns out to be $f(\tilde{\phi}^{(0)}) = -\frac{\gamma}{N} \sum_{\beta=1}^N \frac{\partial W(\phi)}{\partial \phi_\beta}$ owing to $\tilde{\phi}^{(0)}$ satisfying the summation rule. Therefore, Eq. (10) becomes

$$\gamma \frac{\partial^2 \tilde{\phi}_\alpha^{(0)}}{\partial \rho^2} = \gamma \frac{\partial W(\phi)}{\partial \phi_\alpha}(\tilde{\phi}^{(0)}) - \frac{\gamma}{N} \sum_{\beta=1}^N \frac{\partial W(\phi)}{\partial \phi_\beta} \quad \forall \alpha \in \{1, 2, \dots, N\}. \quad (11)$$

However, this is the exact same requirement as obtained in the leading order local analysis of Eq. (1), in Ref. [15]. That means, the same equations, analysis, and the conclusions apply, as far as the leading order is considered, irrespective of whether the τ -formulation is interpolation type or of the Steinbach type. This will also be true for the local analysis pertaining to the junctions, and hence, the force balance conditions have to be fulfilled even in the Steinbach model simulations. That is, for a triple junction, even the Steinbach's model should capture the Young's law in the limit of vanishing interface width. In contrast, the asymptotic analysis of Eq. (1) corresponding to the later orders does not continue to carry over to Eq. (8), the implications of which will be revisited in a while.

Strikingly, redoing the simulations but with the Steinbach form of τ -formulation leads to a better and faster recovery of the triple junction angles as evident from Table 14. Even in the case of higher driving forces, i.e., the parameter set corresponding to Table 16, it is seen that the Steinbach implementation is the superior one. That is, not only does it outperform harmonic mobility interpolation but even the arithmetic one. This state of things may give the impression that Steinbach's formulation, after all, might be the desired full-fledged solution unlike the arithmetic or harmonic ones which are only better under certain special circumstances. However, this is not the case as established by the results for the setup of Fig. 9. Here, the phase

Table 16
 Simulations of Table 14 reperformed but with 10 times larger driving force, i.e, with $f_1 = 2.0$, $f_2 = 0.0$ and $f_3 = 0.0$.

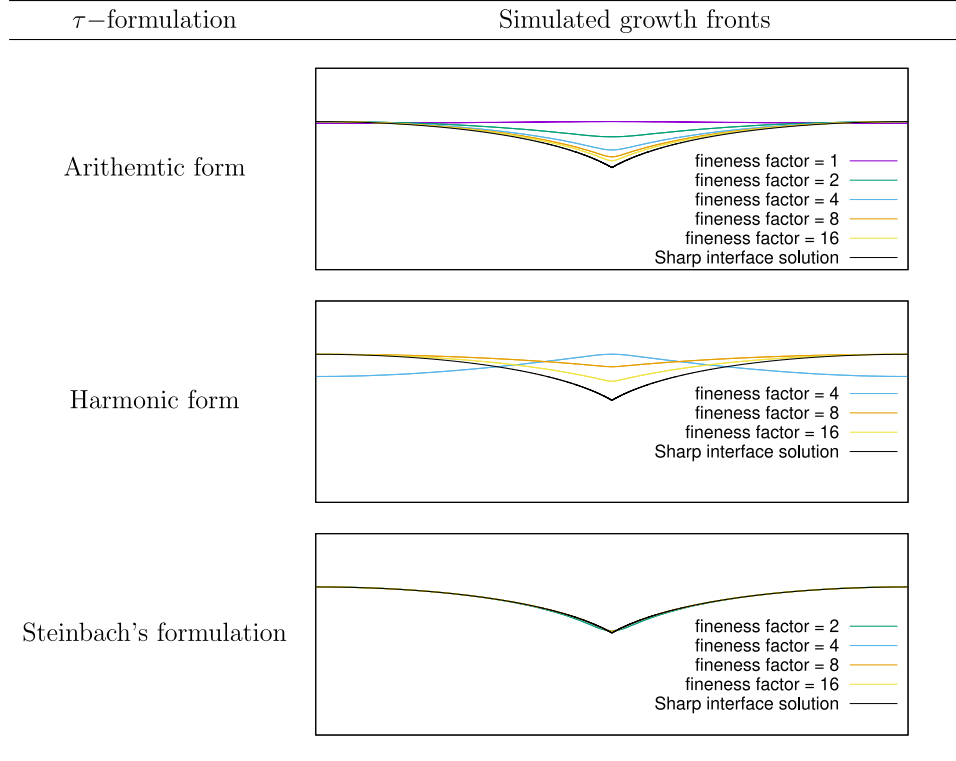


Table 17
 Steady-state angles and speeds recovered for the growth fronts of Table 16.

Fineness factor	Speed recovered with		
	Arithmetic form	Harmonic form	Steinbach's formulation
1	0.01175377	Unstable	Unstable
2	0.01055376	Unstable	0.01438601
4	0.01011871	0.01031806	0.01353602
8	0.00996935	0.01002834	0.01326541
16	0.00991464	0.00993977	0.01316515
Sharp interface theory predicted speed			0.00987556

Table 18
 Table showing a parameter set used for the study of three phase evolution within the setup of Fig. 9.

f_1	f_2	f_3	γ	$\tau_{12} = \tau_{13}$	τ_{12}	N_x	N_y	Δx	Δt	ϵ	$W(\phi)$
0.0	1.0	0.0	1.0	100.0	1.0	64	40	0.5	$0.2(\Delta x)^2$	$5.0\Delta x$	$W^T(\phi)$

ϕ_2 has higher bulk energy compared to the other two phases, and hence the latter have a driving force to eat up the former. However, the mobilities of the interfaces formed by the ϕ_1 phase are 100 times smaller than the one between ϕ_2 and ϕ_3 . As a result, the former barely move, and the interfacial motion is predominantly as indicated by the arrow in the figure. A sequence of simulation images verifying this is presented in Fig. 10. With the initial filling as in Fig. 9, and with the parameter set of Table 18 considered as the base resolution, simulations are performed employing the arithmetic, harmonic and Steinbach forms of τ -implementation for various interface thicknesses. The prescription of $\epsilon = 5.0 \times \Delta x$ is utilized to take advantage of the faster downsizing of the interface width it offers. The recovered results are as indicated in Fig. 11 where the $\phi_2 = 0.5$ contours are plotted after appropriate normalization.

As per the asymptotic analysis requirements, a $120^\circ - 120^\circ - 120^\circ$ angle breakdown is expected due to all the interfacial energies being the same. Whereas, in the arithmetic simulations, as before, a pinning effect is felt, while the Steinbach case reproduced a highly mobile triple junction leading to an almost retention of the originally imposed right angle between the solid–solid and the solid–liquid interfaces. Only the harmonic interpolation stayed close to the theoretically predicted behavior. On increasing the resolution, both the arithmetic and Steinbach profiles changed tending more and more closer to those of the harmonic form, which remained almost the same as the low resolution one and close to the asymptotic requirement. At still higher resolutions, effects pertaining to the problematic $\epsilon \propto \Delta x$ selection began to set in (not shown).

Thus, it is demonstrated that the Steinbach's method, in actuality, is not the all encompassing solution to the problem of finding a τ -formulation that is not too restrictive with regard to the interface width. Furthermore, while this is in relation to the recovery of the interfacial configuration at the junctions, the kinetics of evolution of binary interfaces is also not recovered as per the Gibbs–Thomson condition. This is a direct consequence of the fact that the leading order behaviors (in the matched asymptotic analyses) of Eqs. (1) and (8) are the same but the higher ones are different, which is also evident from the reported simulated steady-state speeds of Tables 15 and 17. Questions like what dynamical law, instead, is recovered and how to adjust it as per the requirement etc., and, even before that, why the bulk energy interpolating forms should necessarily be linear (i.e., $g_\alpha(\phi) = \phi_\alpha$) when borrowing Steinbach's form of equations, are beyond the scope of this work, and hence are not delved into further.

Whatever may be the state of such other details, the takeaway is that the hunt for a universal τ -formulation is far from over and remains to be continued.

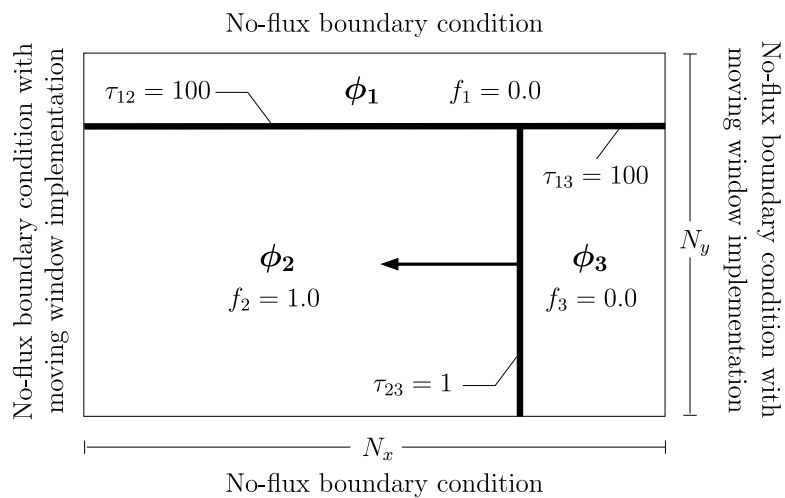


Fig. 9. A simulation setup used for the study of three phase growth. The growth direction is as depicted by the arrow and accordingly is the implementation of the shifting window.

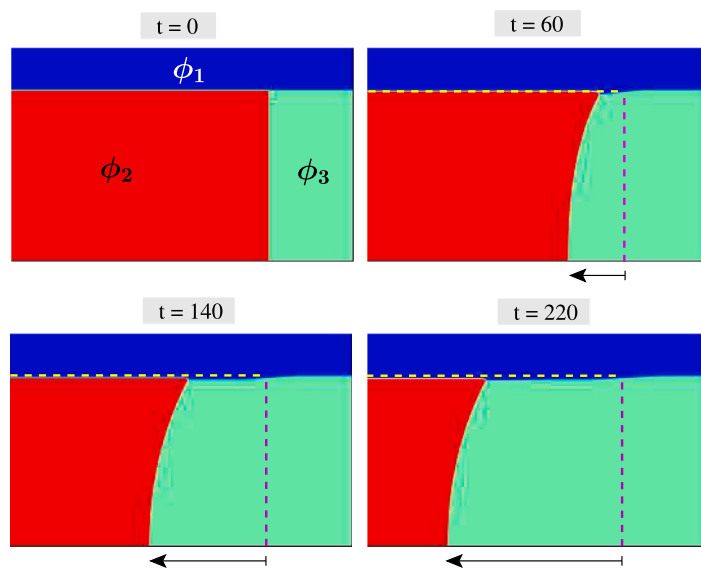


Fig. 10. A sequence of simulation images illustrating the general growth tendency of the three phase system indicated in Fig. 9.

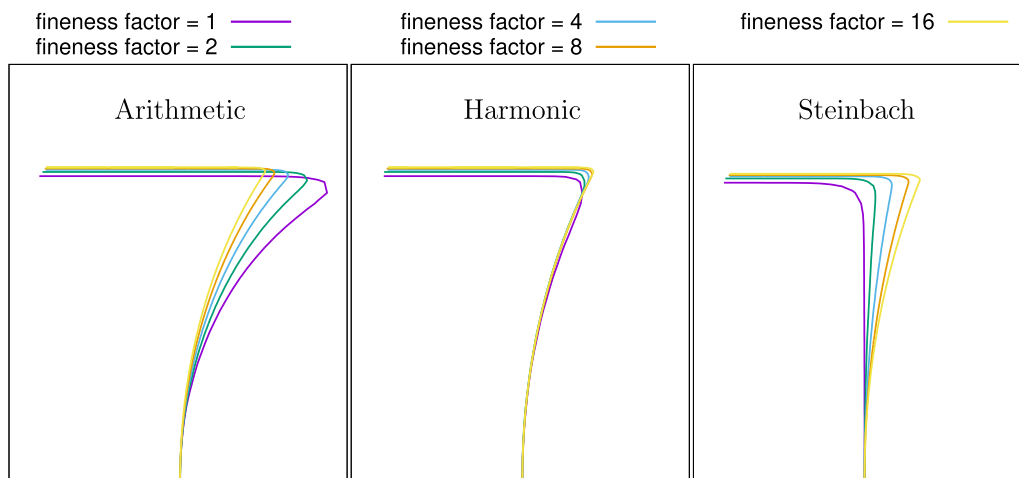


Fig. 11. Simulated $\phi_2 = 0.5$ contours indicating the slow convergence of the arithmetic and Steinbach formulations compared to the harmonic τ -interpolation for the setup of Fig. 9 and the base resolution parameter set listed in Table 18.

5. Summary and conclusion

In Ref. [14], matched asymptotic analysis is performed on an isotropic grain-growth model to uncover the vanishing interface-width limit behavior of binary interfaces, which is then verified numerically. The analysis is furthered in Ref. [15] to determine the limiting kinetics of junction points and the interfacial configuration in their neighborhoods. However, the numerical verification is left unperformed which is commenced in the current article.

First of all, simple numerical analysis exposed that the popular prescription for conducting interface-thickness reduction studies, namely interface-width proportional to the grid discretization ($\epsilon \propto \Delta x$), has to be revised. It has to be replaced with $\epsilon \propto (\Delta x)^p$ with $p < 2/3$. This means that the numerical recovery of asymptotic limit is a far more expensive procedure than previously imagined. Next, while Ref. [14] highlighted the void existing due to the absence of a multi-well formulation capable of handling unequal interfacial energies, the current work identified a new one in the absence of a mobility formulation non-restrictive with regard to the interface widths.

So far in the literature, when a deviation from Young's law is observed, it is often thought to be the final property of the employed phase-field model [16–18]. However, the current article demonstrates that it could very well be an outcome of larger interface widths, reducing which, the results indeed converge onto the sine law, which is also the asymptotics' prediction. Although we have checked this explicitly only for the simplest representative (isotropic grain growth) model, we strongly believe the same behavior would result for the models of Refs. [16–18] because of their similarity. The reason for the sluggish convergence is identified to be the arithmetic form of interpolation of the inverse mobilities, which is the most common choice (although not for any particular reason, but rather as a continued practice). Replacing it with a harmonic form or Steinbach's mobility formulation solved the problem for the setup at hand, but worsened the rate of convergence for other initial fillings and parameter sets. In fact, for each of the three mobility formulations considered, namely Arithmetic, Harmonic, and Steinbach, a setup is identified for which the one in question fails and the other two fare relatively well. That means, a mobility formulation which is universally efficient is yet to be discovered.

The numerical verification of the asymptotics' predicted junction dynamics conducted in the current article is just the beginning. Only the retrieval of Young's law for triple points is verified, and that too for symmetric systems in steady-state. However, the matching analysis' predictions of Ref. [15] are far more wider than that, and touch upon many other aspects of junction evolution. According to them, a force-balance condition has to hold for any junction (triple point or higher order point) in stable motion. Also, like in the case of binary interfaces, a kinetics law governing the instantaneous velocity of motion is also uncovered for junctions. The curvatures of the involving interfaces, their energies and mobilities, and even the bulk energies of the phases feature in it. This law, however, is not yet tested by us directly. The verifications that are currently presented are only by way of an indirect comparison as what is explicitly tested is the agreement of the steady-state motion of the full fronts with the analytical solutions. We plan to carry out a direct validation in an upcoming article not only for triple points but also for higher order junctions. Furthermore, this will be done even for junctions in asymmetric systems and not in steady-state. The next and most important step after that would be to extend the program of 'performing asymptotics and verifying the predictions' to the diffusion-coupled multi-phase-field models.

CRedit authorship contribution statement

E.S. Nani: Conceptualization, Formal analysis, Investigation, Methodology, Software, Validation, Visualization, Writing – original draft, Writing – review & editing. **Britta Nestler:** Funding acquisition, Project

administration, Resources, Software, Supervision, Writing – review & editing.

Declaration of competing interest

The authors declare the following financial interests/personal relationships which may be considered as potential competing interests: Sumanth Nani Enugala reports financial support was provided by German Research Foundation. Johannes Hoetzer reports financial support was provided by German Research Foundation. If there are other authors, they declare that they have no known competing financial interests or personal relationships that could have appeared to influence the work reported in this paper.

Data availability

No data was used for the research described in the article.

Acknowledgments

The authors gratefully acknowledge the funding by the German Research Foundation (DFG) through grant number NE822/31-1 (Gottfried-Wilhelm-Leibniz prize). They further thank Dr. Ing. Amol Subhedar for encouraging us to pursue the analysis of Section 3 after providing a rough version of the starting point.

Appendix. Sharp interface treatment of three-grain evolution within the setup of Fig. 1

The growth front's shape and speed at the steady state are to be determined given its mobility τ , energy γ and driving force Δf .

The law governing the interfacial evolution is

$$\tau v_n = \Delta f - \gamma \kappa \quad (\text{A.1})$$

where v_n is the normal velocity, and the same sign convention as in the local analysis of binary interfaces of Ref. [14] is used for curvature κ .

Since there is a mirror symmetry in the system about the $\phi_2 - \phi_3$ interface, only the right side grain's evolution is explicitly worked on. Let us position the coordinate system such that the origin coincides with the triple point. Since the interface profile is assumed to be always expressible as graph of a function, various points on it can be identified using just the abscissa x . Therefore, Eq. (A.1), re-written highlighting this, would read

$$\tau v_n(x) = \Delta f - \gamma \kappa(x) \quad \forall 0 < x \leq l$$

where l is the width of the growing grain ϕ_3 . Since the front moves upwards without changing its shape, it can be readily shown that this equation reduces to

$$\frac{\tau v}{\sqrt{1 + \left(\frac{dy}{dx}\right)^2}} = \Delta f - \gamma \kappa(x) \quad \forall 0 < x \leq l \quad (\text{A.2})$$

where v is the steady-state speed.

That means, the problem statement is to find a $y(x)$ and a v satisfying

$$\frac{-\frac{d^2y}{dx^2}}{\left(\sqrt{1 + \left(\frac{dy}{dx}\right)^2}\right)^3} + \frac{\tau}{\gamma} \frac{v}{\sqrt{1 + \left(\frac{dy}{dx}\right)^2}} - \frac{\Delta f}{\gamma} = 0 \quad (\text{A.3})$$

in the interval $(0, l]$ subject to the boundary conditions

$$\frac{dy}{dx}(x=0) = \tan \theta_1 \quad \text{and} \quad (\text{A.4})$$

$$\frac{dy}{dx}(x=l) = 0 \quad (\text{A.5})$$

where θ_1 is the angle made by the $\phi_1 - \phi_3$ interface with the horizontal.

The second of the above conditions is realized in the phase-field simulations due to implementation of no-flux boundary conditions in the lateral directions [12].

The solution is obtained in the following manner: Substituting $m = dy/dx$ in Eq. (A.3) yields

$$\frac{-\frac{dm}{dx}}{(1+m^2)^{3/2}} + \frac{a}{(1+m^2)^{1/2}} - b = 0 \quad (\text{A.6})$$

where a and b are used to denote $\tau v/\gamma$ and $\Delta f/\gamma$, respectively. If $\theta(x)$ is the angle made by the interface with the horizontal at x , then by definition, $m = \tan \theta$. This would imply

$$\frac{dm}{dx} = \sec^2 \theta \frac{d\theta}{dx}. \quad (\text{A.7})$$

Substituting Eq. (A.7) in Eq. (A.6) leads to

$$-\frac{\sec^2 \theta}{(\sec^2 \theta)^{3/2}} \frac{d\theta}{dx} + \frac{a}{(\sec^2 \theta)^{1/2}} - b = 0 \quad (\text{A.8})$$

$$\Rightarrow -\cos \theta \frac{d\theta}{dx} + a \cos \theta - b = 0 \quad (\text{A.9})$$

$$\Rightarrow \frac{a \cos \theta}{(a \cos \theta - b)} \frac{d\theta}{dx} = a \quad (\text{A.10})$$

$$\Rightarrow \frac{d\theta}{dx} + \frac{b}{(a \cos \theta - b)} \frac{d\theta}{dx} = a. \quad (\text{A.11})$$

Substituting $\cos \theta = \frac{(1-\tan^2 \frac{\theta}{2})}{(1+\tan^2 \frac{\theta}{2})}$ and rearranging yields

$$\frac{d\theta}{dx} + \frac{b \sec^2 \frac{\theta}{2} \frac{d\theta}{dx}}{(a-b-(a+b)\tan^2 \frac{\theta}{2})} = a. \quad (\text{A.12})$$

Let $\tan \frac{\theta}{2} = p$ for the second summand on the l.h.s. This transforms Eq. (A.12) to

$$\frac{d\theta}{dx} - \frac{2b}{b+a} \frac{dp/dx}{\left\{ p^2 + \left(\sqrt{\frac{b-a}{b+a}} \right)^2 \right\}} = a. \quad (\text{A.13})$$

Integrating Eq. (A.13) gives

$$\theta - \frac{2b}{b+a} \sqrt{\frac{b+a}{b-a}} \tan^{-1} \left(\sqrt{\frac{b+a}{b-a}} \tan \frac{\theta}{2} \right) = a(x+c) \quad (\text{A.14})$$

where c is the integration constant which can be easily shown to equal $-l$ by considering the equation for $x = l$ and using the corresponding boundary condition. Thus, the angle made by the interface with the horizontal at every x is given by

$$\theta - \frac{2}{\sqrt{1-\left(\frac{a}{b}\right)^2}} \tan^{-1} \left(\sqrt{\frac{1+\frac{a}{b}}{1-\frac{a}{b}}} \tan \frac{\theta}{2} \right) = \frac{a}{b} b(x-l). \quad (\text{A.15})$$

Note that the unknown v is in a/b and it can be determined by considering the above equation for $x = 0$. Expressing a/b in closed form from the above may not be possible, however, using numerical techniques, it can be determined for any given θ_1 up to desired level of accuracy. The free online Wolfram Mathematica tool is used to evaluate a/b for the problems considered in the present article. Once it is available, the interface profile $y(x)$ can be obtained from $\theta(x)$ using numerical integration. The same route is taken in obtaining all the sharp-interface profiles of the current work.

References

- [1] W. Eckhaus, *Asymptotic Analysis of Singular Perturbations*, Elsevier, 2011.
- [2] R.E. O'Malley Jr., *Introduction to Singular Perturbations*, Tech. Rep., 1974.
- [3] M.H. Holmes, *Introduction to Perturbation Methods*, Vol. 20, Springer Science & Business Media, 2012.
- [4] G. Caginalp, An analysis of a phase field model of a free boundary, *Arch. Ration. Mech. Anal.* 92 (3) (1986) 205–245.
- [5] G. Caginalp, Stefan and Hele-Shaw type models as asymptotic limits of the phase-field equations, *Phys. Rev. A* 39 (11) (1989) 5887.
- [6] A. Karma, W.-J. Rappel, Quantitative phase-field modeling of dendritic growth in two and three dimensions, *Phys. Rev. E* 57 (4) (1998) 4323.
- [7] R.F. Almgren, Second-order phase field asymptotics for unequal conductivities, *SIAM J. Appl. Math.* 59 (6) (1999) 2086–2107.
- [8] A. Karma, Phase-field formulation for quantitative modeling of alloy solidification, *Phys. Rev. Lett.* 87 (11) (2001) 115701.
- [9] B. Echebarria, R. Folch, A. Karma, M. Plapp, Quantitative phase-field model of alloy solidification, *Phys. Rev. E* 70 (6) (2004) 061604.
- [10] M. Ohno, K. Matsuura, Quantitative phase-field modeling for dilute alloy solidification involving diffusion in the solid, *Phys. Rev. E* 79 (3) (2009) 031603.
- [11] M. Ohno, T. Takaki, Y. Shibuta, Variational formulation of a quantitative phase-field model for nonisothermal solidification in a multicomponent alloy, *Phys. Rev. E* 96 (3) (2017) 033311.
- [12] L. Bronsard, F. Reitich, On three-phase boundary motion and the singular limit of a vector-valued Ginzburg-Landau equation, *Arch. Ration. Mech. Anal.* 124 (4) (1993) 355–379.
- [13] A.A. Wheeler, G. McFadden, W. Boettinger, Phase-field model for solidification of a eutectic alloy, *Proc. R. Soc. Lond. Ser. A Math. Phys. Eng. Sci.* 452 (1946) (1996) 495–525.
- [14] E.S. Nani, B. Nestler, Asymptotic analysis of multi-phase-field models: A thorough consideration of binary interfaces, *Phys. Rev. E* 105 (2022) 014802.
- [15] E. Nani, B. Nestler, Asymptotic analysis of multi-phase-field models: a thorough consideration of junctions, *Physical Review E* 107 (2) (2023) 024803.
- [16] S. Ghosh, A. Karma, M. Plapp, S. Akamatsu, S. Bottin-Rousseau, G. Faivre, Influence of morphological instability on grain boundary trajectory during directional solidification, *Acta Mater.* 175 (2019) 214–221.
- [17] F. Wendler, A. Okamoto, P. Blum, Phase-field modeling of epitaxial growth of polycrystalline quartz veins in hydrothermal experiments, *Geofluids* 16 (2) (2016) 211–230.
- [18] N. Prajapati, A. Abad Gonzalez, M. Selzer, B. Nestler, B. Busch, C. Hilgers, Quartz cementation in polycrystalline sandstone: Insights from phase-field simulations, *J. Geophys. Res.: Solid Earth* 125 (2) (2020) e2019JB019137.
- [19] I. Steinbach, F. Pezzolla, B. Nestler, M. Seeßelberg, R. Prieler, G.J. Schmitz, J.L. Rezende, A phase field concept for multiphase systems, *Physica D* 94 (3) (1996) 135–147.